Diverging Polymer Acoustic Lens Design for High-Resolution Row-Column Array Ultrasound Transducers

Audoin, Melanie; Salari, Ali; Tomov, Borislav Gueorguiev; Pedersen, Kasper Fløng; Jensen, Jorgen Arendt; Thomsen, Erik Vilain

Published in:
IEEE Transactions on Ultrasonics, Ferroelectrics, and Frequency Control

Link to article, DOI:
10.1109/TUFFC.2023.3327567

Publication date:
2024

Document Version
Peer reviewed version

Diverging Polymer Acoustic Lens Design for High-Resolution Row-Column Array Ultrasound Transducers

Mélanie Audoin, Ali Salari, Borislav Gueorguiev Tomov, Kasper Fløng Pedersen, Jørgen Arendt Jensen, and Erik Vilain Thomsen

Department of Health Technology, Technical University of Denmark, DK-2800 Kgs. Lyngby, Denmark

***Abstract*—Spherical diverging acoustic lenses mounted on flat 2D Row-Column Addressed (RCA) ultrasound transducers have shown the potential to extend the Field of View (FOV) from a rectilinear to a curvilinear volume region and thereby enable 3D imaging of large organs. Such lenses are usually designed for small aperture low-frequency transducers, which have limited resolution. Moreover, they are made of off-the-shelf pieces of materials, which leaves no room for optimization. We hypothesize that acoustic lenses can be designed to fit high-resolution transducers and they can be fabricated in a fast, cost-effective, and flexible manner using a combination of 3D printing and casting or CNC machining techniques. These lenses should increase the FOV of the array while preserving the image quality. In this work, such lenses are made in concave, convex, and compound spherical shapes, and from thermoplastics and thermosetting polymers. Polymethylpentene (TPX), Polystyrene (PS), Polypropylene (PP), Polymethyl methacrylate (PMMA), Polydimethylsiloxane (PDMS) and Room-temperature-vulcanizing silicone (RTV) diverging lenses have been fabricated and mounted on a 128+128 6 MHz RCA transducer. The performances of the lenses have been assessed and compared in terms of FOV, Signal to Noise Ratio (SNR), bandwidth, and potential artefacts. The largest FOV (24.0°) is obtained with a 42.64 mm radius PMMA-RTV compound lens, which maintains a decent fractional bandwidth (53%) and SNR at 6 MHz (-9.1 dB amplitude drop compared to the unlensed transducer). The simple PMMA TPX, PS, PP, PDMS and RTV lenses provide a FOV of 12.2°, 6.3°, 8.1°, 11.7°, 0.6° and 10.4°, a fractional bandwidth of 97%, 46%, 103%, 46%, 97%, 53% and 49%, and an amplitude drop of -5.2 dB, -4.4 dB, -2.8 dB, -15.4 dB, -6.0 dB and -1.8 dB respectively. This work demonstrates that thermoplastics are suitable materials for fabricating low-attenuation convex diverging lenses for large-aperture, high-frequency 2D transducers. This is highly desired to achieve high-resolution volumetric imaging of large organs.**

I. Introduction

Row-Column Addressed (RCA) ultrasound transducers provide an efficient way of performing high resolution 3D ultrasound imaging [1]–[7]. RCA arrays are made of two perpendicular 1D-arrays and use rows to transmit and columns to receive – or the opposite. The imaging area corresponds to the overlap between the transmit and receive area, which effectively corresponds to the footprint of the transducer. This rectilinear imaging area strongly limits the application of RCA transducers for anatomical imaging of large organs for two reasons. First, the current largest commercial RCA probes ($2.5\,\mathrm{cm}^2$, 128+128 Vermon, or $3.5\,\mathrm{cm}^2$ 256+256 [6]) are significantly smaller than a human liver or kidney ($12\,\mathrm{cm}$ x $6\,\mathrm{cm}$). Secondly, for 3D cardiac imaging, the presence of the ribs prevents the use of large probes and instead requires curvilinear imaging. To obtain a curvilinear Field of View (FOV), one common solution is to use convex arrays. Commercial convex linear arrays provide a FOV from 60° to 100° [8]–[11]. However, contrary to linear arrays, manufacturing a 2D RCA array in a double-convex shape would be complicated due to the in-built elongated crossed-element structure. A more simple method to increase the FOV is to use a diverging acoustic lens [12]–[15]. Despite the lens introducing additional ultrasound attenuation in the propagation way, this is often the preferred solution for 2D RCA arrays which can overcome this drawback by emitting much more energy than linear arrays. Such 2D diverging lenses are usually made in a convex or concave spherical shape as shown in Fig. 1 and provide a FOV from around 20° to 40°.

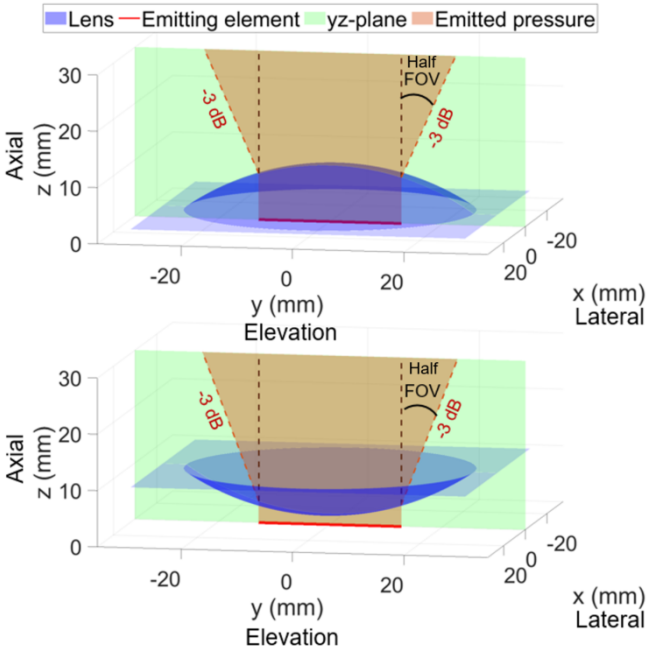

Fig. 1. Representation of a spherical convex lens (top) or concave lens (bottom). The lens is shown in blue. The lens is placed on top of the array and one of the emitting elements is shown in red. The pressure emitted through the lens is shown in orange for the elevation plane (green). The sound is spread further out compared to the case without a lens (black dashed line). The half FOV is defined as the angle between the black and red dashed lines.

However, these lenses are currently designed for transducers operating at low frequency ($< 5\,\mathrm{MHz}$) and having a small aperture width ($< 15\,\mathrm{mm}$), which severely limits their resolution. Indeed, the axial resolution of an ultrasound image is directly proportional to the wavelength λ and the lateral resolution is determined by the Full Width Half Maximum (FWHM) of the Point Spread Function (PSF), which is given by $FWHM = \lambda.F_{\#} = \lambda.\frac{\text{Depth}}{\text{Aperture width}}$ [4]. Therefore, large aperture high-frequency transducers are highly desirable to achieve high-resolution imaging. Yet, lensing such arrays becomes challenging for two reasons. First, the radius of curvature of the lens has to increase considerably to cover the whole array, which severely limits the divergence of the lens. Secondly, the choice of lens material becomes restricted to those having a low frequency-dependent attenuation coefficient to preserve the sensitivity and bandwidth at high frequencies. Therefore, both the lens geometry and material require a thorough optimization to obtain a large FOV with a high-resolution transducer. The present study focuses on spherical lenses and aims to investigate the potential and performances of different polymer materials for making diverging lenses for large aperture high frequency RCA transducers.

Acoustic lenses are commonly built in thermosetting polymers, which include epoxy, silicone, vulcanized rubber, and polyurethane [13], [15]–[18]. Lenses made of thermosets can easily be manufactured using a casting process, however, these materials carry two serious limitations when considering their value for clinical studies. First, these thermosets have a highly frequency-dependent acoustic attenuation, which compromises the contrast and resolution of the image. This effect becomes particularly challenging for transducers having a high center frequency, as the attenuation increases exponentially with frequency for such materials in the MHz range. These lens materials are therefore not suitable for making high-resolution images with high-frequency transducers. Secondly, the speed of sound in silicone and rubbers is lower than in the imaging medium, which implies that the surface of the lens needs to be concave to have a diverging effect. This prevents their use for clinical studies as the space between the concave surface of the lens and the patient's skin can too easily trap air. Thus, compound lenses have been developed to obtain a flat surface by stacking a convex lens on top of a concave one to obtain a flat surface. Still, the second material is often another strongly attenuating thermoset like urethane [13] or epoxy [15].

The existing acoustic lenses carry limitations on their clinical applicability to high-resolution and large volumetric ultrasound imaging. Therefore, it becomes necessary to explore a new range of materials for making diverging convex ultrasound lenses for large aperture and high-frequency transducers. In this paper, a process flow for designing, manufacturing, and characterizing 3D diverging acoustic lenses in a wide range of geometries and materials is presented. The work shows how this process enables the fabrication of lenses in a fast, cost-effective, and flexible manner. The performance and potential applications and limitations of the different lenses are also discussed in detail.

The paper is organized as follows: In Section II the method to design the lenses is explained, in Section III, the fabrication and characterization of the lenses are described. Then, in Section IV, the results are presented and discussed. Finally, in Section V, the conclusion is given.

II. Design

When designing a diverging lens for a specific RCA transducer, both the lens geometry and material need to be chosen so that the FOV is maximized and the image quality is preserved. A figure of merit is developed to facilitate the design process with regard to the two aforementioned optimization criteria.

First, the FOV of a diverging lens is estimated using the thin lens model [19]. The elongated elements of a RCA array emit cylindrical waves and therefore the sound does not propagate further than the element edge in the elevation direction. However, the sound beam can be diverged, just like in optics, by adding an object having a curved surface along this direction and made of a material with an appropriate acoustic refractive index. Therefore, these 3D diverging lenses are designed in a spherical shape to diverge the sound beam from both the row and column elements of a flat RCA array as shown in Fig. 1. The amount of divergence is quantified by the FOV, which describes the angular spread of energy in the imaging medium. The thin lens model provides a simple estimation of the FOV of a lensed array based on the paraxial condition assumption but disregards the thickness and losses introduced by the lens [20]. The FOV is given by [19]:

$$FOV = 2\cot^{-1}\left(-\frac{2}{L_t}F\right) = 2\cot^{-1}\left(\frac{2}{L_t}\frac{R}{n_a - 1}\right) \tag{1}$$

where the FOV is the two-sided field of view, $F = \frac{R}{1-n_a}$ the focal distance - negative for a diverging lens, L_t the length of the emitting elements, R the radius of curvature of the lens - positive for a convex lens and n_a is the acoustic refractive index:

$$n_a = \begin{cases} \frac{v_l}{v_m}, & \text{if } v_l \geq v_m \\ \frac{v_m}{v_l}, & \text{if } v_l \leq v_m \end{cases} \tag{2}$$

where v_m, and v_l denote the speed of sound in the imaging medium and lens material, respectively.

Equations (1) and (2) show that when using a material in which the speed of sound is higher than in the imaging medium ($v_l > v_m$), a diverging lens is obtained if the radius of curvature is positive ($R > 0$), i.e., the lens is convex. Alternatively, when using a material for which $v_l < v_m$, the lens is diverging only if it has a concave shape ($R < 0$).

It also shows that to maximize the FOV, R should be minimized and n_a maximized. However, the lens should at least circumscribe the array, and therefore the radius R is constrained by $R \geq L_t/\sqrt{2}$. To maximize n_a the lens should be made of a material in which the speed of sound is very different from the one in the imaging medium, $v_m = 1540\,\mathrm{m\,s^{-1}}$ for body tissue.

Secondly, the lens should preserve the image quality measured in terms of Signal to Noise Ratio (SNR), resolution, and absence of artefacts.

The SNR and resolution are directly related to the shape of the impulse response. The amplitude of the transmit signal determines the SNR. The frequency impulse response spectrum determines the spatial resolution since it is proportional to the wavelength λ.

The amplitude of the transmitted wave is affected by the attenuation occurring inside the lens and by the refraction at its boundary. The transmitted power after propagation through a lossy material is given by:

$$T_l = 10^{-\alpha(f)*H/10}, \text{ with } \alpha(f) = \alpha_0 + \alpha_f * (f - f_0) \quad (3)$$

with T_l being the transmission coefficient, H the thickness of the material [cm], f the frequency [MHz], α_0 the attenuation coefficient [$\mathrm{dB\,cm^{-1}}$] of the material at some reference frequency f_0 and α_f the frequency dependant attenuation coefficient of the material [$\mathrm{dB\,cm^{-1}\,MHz^{-1}}$].

The transmitted power after partial refraction at the boundary is given by:

$$T_r = \frac{4Z_lZ_m}{(Z_m + Z_l)^2} \quad (4)$$

with T_r being the transmission coefficient, Z_m and Z_l being the acoustic impedance of the imaging medium and lens material respectively [MRayl]. The acoustic impedance is given by $Z = \rho v$ where ρ is the density and v is the speed of sound.

The total transmitted power is then given by the product of the two transmission coefficients :

$$T_{tot} = T_l * T_r \quad (5)$$

To maximize the amplitude of the transmitted wave, (3) shows that the lens should be as thin as possible and that the material should have a small attenuation coefficient.

The thickness of a lens that covers the entire array is given by the chord height of its arc and is related to the other geometrical parameters through:

$$H(R, L_t) = R - \sqrt{R - \frac{L_t^2}{2}} \quad (6)$$

where H is the chord height, R the radius of curvature and L_t the length of the transducer elements.

It should also be noted that T_l depends exponentially on the frequency. This parameter influences the shape of the frequency impulse response and causes a down-shift of the center frequency and a reduction in the bandwidth [16], [21]. The attenuation coefficient is also of the foremost importance for a high-frequency transducer as the signal can be completely damped at these frequencies.

Equation 4 shows that the transmitted wave power increases when the ratio Z_m/Z_l is close to 1, which imposes a constraint on the density and speed of sound in the chosen material.

Having a good impedance match between the lens and imaging medium is also crucial to avoid imaging artefacts. Indeed, if the wave is strongly reflected inside the lens it will lead to secondary echoes, which appear as reverberations in the ultrasound image [14], [16]. To limit this phenomenon, the power ratio of the reflected to transmitted wave, ν, should be minimized. For a normally incident wave, it is given by

$$\nu = \frac{(Z_m - Z_l)^2}{4Z_mZ_l}, \quad (7)$$

which shows that to keep ν below $-30\,\mathrm{dB}$ in body tissue ($Z_m = 1.54$ MRayl), the impedance of the lens material should lie between $[1.1 - 2.2]$ MRayl.

Transducer properties

Name	**Vermon RC**
Type	2D PZT RCA
Number of elements	128 + 128
Footprint	25.6 x 25.6 mm^2
Center frequency	6 MHz
Element length	25.6 mm
Pitch	0.2 mm
Kerf	0.02 mm
Apodization	None

TABLE I
TRANSDUCER PROPERTIES

III. METHODS

A. Design

Based on the framework developed in Section II, the lens design is optimized in terms of material and geometry for a 128+128 RCA transducer (Vermon) having a $25.6\,\mathrm{mm^2}$ footprint and a $6\,\mathrm{MHz}$ center frequency, as described in Table I. Fig. 2 shows the theoretical FOV against the transmitted power through the lens as derived by (1) and (5) for different polymer materials. Each line shows the FOV as a function of the transmitted power for R going from 20 to $80\,\mathrm{mm}$. The best design should simultaneously maximize the FOV and the transmitted power. This graph is used as a figure of merit for designing the lenses. The fabricated lenses are represented by a star in Fig. 2 and correspond to a decision to make a trade-off between preserving the signal strength and increasing the FOV. It should be noted that the fabricated lenses are $4\,\mathrm{mm}$ thick, and therefore, the experimental results might differ from those derived with this model based on the thin lens approximation. The fabricated lens characteristics are summarized in Table II.

B. Material characterization

The lens polymer materials are characterized acoustically using a pulse transmission method described by Wang et al. [22]. A flat rectangular sample of known thickness is placed in a water tank between two aligned hydrophones (Optel). One hydrophone emits a 3 cycles sinusoid signal and the other one receives using an oscilloscope (Tektronix) and PicoScope (PicoScope 5000 series). The measurement compares the signal captured by the receiving transducer with and without the presence of the sample. The changes in the delay and amplitude of the signal are related respectively to the speed of sound and attenuation in the material.

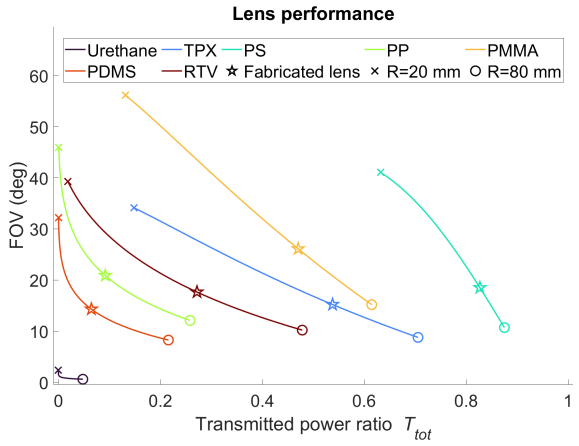

Fig. 2. Evolution of the FOV as a function of the transmitted power ratio for different geometries and materials. Material parameters are found in Table II. Decreasing the radius increases the FOV but also the thickness of the lens and consequently the attenuation. The selected radius $R = 42.64\,\mathrm{mm}$ is represented by a star and corresponds to a thickness of $H = 4\,\mathrm{mm}$ when covering the entire array.

The longitudinal speed of sound and attenuation is measured in the 3-7 MHz range. The speed of sound is found to be constant over the MHz frequency range, and the attenuation coefficient can be extrapolated linearly for higher frequencies. The density is found by measuring the mass and volume of a rectangular piece of material. The results can be found in Table II.

C. Fabrication

The lenses are fabricated using two different methods depending on the type of polymer that needs to be used.

1) Thermoset lens: Thermosetting polymers refer to materials that remain permanently solid after curing. The curing reaction involves the formation of irreversible cross-linking bonds. Low-volume production of these polymers can be most easily achieved using casting techniques. The thermosets used for lens fabrication in this work include Polydimethylsiloxane (PDMS) (Sylard, PDMS170) and Room-temperature-vulcanizing silicone (RTV) (Momentive, RTV615). The polymer is cast by first mixing the two liquid parts of the uncured material using a centrifuge (Thinky ARE-250). Then, the mixture is poured into the lens mould where it is degassed under vacuum until there are no more visible air bubbles. Finally, the lens is cured overnight at $45\,^{\circ}\mathrm{C}$. The lens mold is 3D printed with a $25\,\mu\mathrm{m}$ voxel resolution SLA printer (Formlabs, Form 3), then polished with a P1200 graded emery cloth and clear coated (Wurth, nitro-alkydal special clear lacquer) to obtain an anti-sticking surface of sub-wavelength roughness. The lens is cast on a frame that can be screwed on a specially designed probe holder as shown in Fig. 3.a). This way, the lenses can be easily mounted and removed from the probe. To ensure adherence of the cast polymer to the frame a thin layer of primer is applied before casting. The primers used are Momentive SS4120 for RTV615 and Dowsil 1200 OS for PDMS170.

2) Thermoplastic lens: Manufacturing of thermoplastics for low-volume production can be achieved with CNC machining. Thermoplastics are usually supplied in the form of pellets or sheets and therefore the thermoplastics lenses are manufactured from a sheet of polymer of about 50x50x6 mm made of Polymethylpentene (TPX), Polystyrene (PS), Polypropylene (PP) or Polymethyl methacrylate (PMMA). The polymer is chosen as pure as possible, e.g. without color additive, which would otherwise increase the attenuation of the material. The piece of polymer is micro-milled using a CNC milling machine (Minitech, Mini-mill/3). Several passes using ball nose end mills from 1 to $0.25\,\mathrm{mm}$ diameter on the spherical surface are executed to ensure a sub-wavelength surface roughness. The lens is milled in a shape that includes the frame that will be screwed onto the array as shown in Fig. 3.b).

3) Compound lens: Compound lenses made of a combination of a thermoset and a thermoplastic material can be fabricated by combining the presented milling and casting techniques. This lens is prepared by first milling the thermoplastic lens and then using this lens as a mold to cast the thermoset lens on top of it. A primer (Momentive SS4120) is applied on the first lens to ensure good bonding between the two stacked lenses. A compound lens made of PMMA and RTV is fabricated and is shown in Fig. 3.c). This combination of materials is chosen to obtain the largest FOV, despite expecting some strong impedance mismatch limitations.

D. Measurements

The lens is mounted on a 128+128 PZT RCA probe (Vermon) having a 25.6x25.6 mm^2 footprint and a $6\,\mathrm{MHz}$ center frequency as shown in Fig. 3.d). The transmit pressure field is mapped using an Onda HGL-0400 hydrophone, Onda HH-2010-100 amplifier, Picoscope 5244D oscilloscope, and using a Verasonics Vantage 256 as the transmit source.

For mapping the transmit pressure, the array emits a two-cycle pulse with all the columns simultaneously, thereby generating a plane wave through the lens. The hydrophone records the pressure at different positions in the elevation plane. The transmit impulse response of the lensed array is obtained by exciting each element separately with 50 coded excitation signals and by measuring the pressure below the excited element at a constant depth of $30\,\mathrm{mm}$. Then, the response signal is cross-correlated with the excitation signal and averaged over all emissions and all elements to obtain the impulse response of the lensed transducer.

Finally, a custom multi-wire phantom is imaged with the lensed arrays. The phantom consists of an assembly of thin metallic wires placed horizontally along the lateral direction (x-axis). The imaging system comprises a 2D RCA array, a lens, and a beamforming method, and changing any of these elements might influence the quality of the image. Consequently, all the phantom images are produced using the same transducer and the same thin-lens based beamformer for convex lensed RCA array developed by Salari et al. [23]. This choice enables a fair comparison between the lenses' imaging performance.

Lens properties

	Property	Units	Lens							
			No lens (Water)	TPX	PS	PP	PMMA	PDMS	RTV	PMMA-RTV
Lens Material	v_l	[m/s]	1480	2123	2340	2460	2713	930	1020	-
	α_0 at $f_0 = 6$MHz †	[dB/cm]	0.0022	10.5	2.0	27.4	7.1	31.0	14.4	-
	α_f †	[dB/cm/MHz]	-	1.9	0.3	3.9	0.9	7.6	3.1	-
	Z	[MRayl]	1.48	1.69	2.42	2.26	3.22	1.30	1.11	-
	n_a	-	1	1.43	1.58	1.66	1.83	1.59	1.45	-
Lens Geometry	Shape	-	-	Convex	Convex	Convex	Convex	Concave	Concave	Compound
	Radius, R	[mm]	-	46.13	46.13	42.64	42.64	42.64	42.64	42.64
	Thickness, H	[mm]	-	4	4	4	4	4	4	4+2
	Chord width	[mm]	-	37.57	37.57	36.06	36.06	36.06	36.06	36.06
FOV	$\text{FOV}_{f\#}$	[deg]	0	9.7	11.2	14.3	14.6	17.7	13.4	25.8
	FOV_{-3dB}	[deg]	0	6.3	8.1	11.7	12.2	0.6	10.4	24.0
Impulse response	Main signal amplitude	[dB]/Ref	0 [Ref]	-4.4	-2.8	-15.4	-5.2	-6.0	-1.8	-9.1
	2^{nd} echo amplitude ‡	[dB]/Main	-15.4 [edg.]	-19.2 [edg.]	-8.6 [refr.]	-16.5 [edg.]	-10.4 [refr.]	-20.9 [edg.]	-16.5 [edg.]	-10.2 [refr.]
	Center frequency f_c	[MHz]	6.25	5.34	6.06	4.80	5.78	4.93	5.62	5.31
	Bandwidth	% of f_c	103	46	103	46	97	53	49	53

† The attenuation coefficient depends on the frequency f as : $\alpha(f) = \alpha_0 + \alpha_f * (f - f_0)$.

‡ The second echo amplitude shows only the largest of the secondary echoes. The nature of this echo is specified as [edg.] for edge wave and [refr.] for refracted wave.

TABLE II
SUMMARY OF THE LENSES PROPERTIES AND CHARACTERIZATION RESULTS.

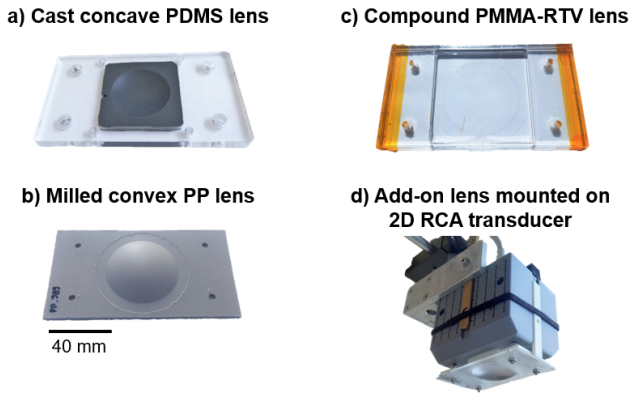

Fig. 3. (a) Concave lens cast in PDMS. (b) Convex lens micro-milled in a sheet of PP. (c) A compound lens made of a stack of a convex PMMA and a concave RTV lens. (d) Add-on lens mounted on the 2D RCA probe using a specially designed holder

IV. Results and Discussion

Several spherical lenses have been successfully fabricated with a suitable radius of curvature R and materials as presented in Table II. They are shown in Fig. 3 along with the lens holder system. The presented process provides an efficient solution for manufacturing tailor-made defocusing lenses for 2D RCA arrays and could easily be applied to fabricate focusing lenses for a linear transducer.

To validate the diverging properties of the lenses, the transmit pressure field is measured in the vertical plane parallel to the emitting elements and passing through the middle of the array as shown in green in Fig. 1.

Fig. 4 shows the maximum pressure field on a linear scale along with the $-3\,\text{dB}$ and $-20\,\text{dB}$ contour lines marked by the black dashed lines. Fig. 4.a) corresponds to the case without a lens and is used as a reference and Fig. 4.b-h) show the field for the different lenses presented in Table II. The larger area inside the black dashed line for the lensed arrays compared to the one without lens shows that the diverging lenses spread the energy in a larger volume as expected.

For the highly attenuating PDMS concave lens, shown in Fig. 4.f), an apodization effect is visible, which translates into a stronger attenuation of the signal at the edges of the array than in its center. This effect is so strong here that the high-pressure field, delimited by the $-3\,\text{dB}$ dashed line, appears restricted to an area below the transducer even more narrow along the elevation axis (y-axis) than without lens. Yet, a large homogeneous pressure field is required for good image quality, so the usability of this diverging lens might be compromised. This effect is less noticeable on Fig. 4.g), which is measured on a RTV concave lens for which the attenuation at $6\,\text{MHz}$ is much smaller ($\alpha = 14.4\,\text{dB}\,\text{cm}^{-1}$ for RTV vs $\alpha = 31.0\,\text{dB}\,\text{cm}^{-1}$ for PDMS). For convex lenses made with medium to highly attenuating materials like TPX, PP and PMMA, shown in Fig. 4.b), d) and e) respectively, a counter-apodization effect can be seen, and the pressure is most strongly attenuated in the center of the array. This is also undesired as it would enhance edge wave artefacts, especially for a non-apodized array like the one used here. A very strongly attenuating material, like PP in Fig. 4.d), completely degrades the SNR ($\alpha = 27.4\,\text{dB}\,\text{cm}^{-1}$ at $f = 6\,\text{MHz}$). For the PMMA-RTV compound lens, in Fig. 4.h), it is seen that the overall field is apodized in a way that the pressure is stronger in the center. This is expected and desired, due to the most attenuating material of the two being the one cast in a concave shape.

To quantitatively compare the performances of the lenses, the FOV is estimated from the measurement of the f-number

This article has been accepted for publication in IEEE Transactions on Ultrasonics, Ferroelectrics, and Frequency Control. This is the author's version which has not been fully edited and content may change prior to final publication. Citation information: DOI 10.1109/TUFFC.2023.3327567

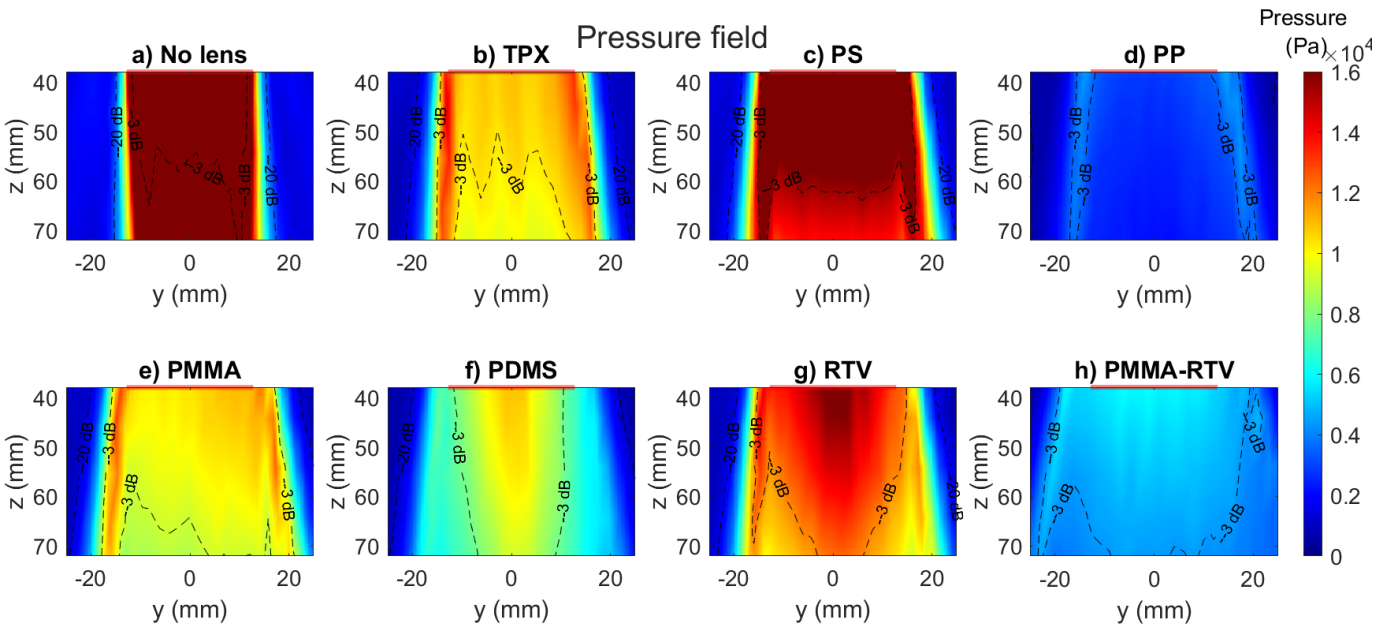

Fig. 4. Transmit pressure field measured for the different lenses presented in Table II. The figure shows the pressure in the vertical plane parallel to the emitting elements and passing through the center of the array, shown in green in Fig.1. The $-3\,\mathrm{dB}$ and $-20\,\mathrm{dB}$ contours are shown as a black dashed line. The array emits a plane wave and lies at $z = 0\,\mathrm{mm}$, i.e. $40\,\mathrm{mm}$ above the image shown here and its spatial extent is shown by a red line to guide the eye. Using a lens spreads the acoustic energy in a bigger volume in the elevation direction (y-axis).

$f_\# = F/L_t$ using (1). The effect of the diverging lens is to apply a varying delay across the transducer, which creates a convex wavefront out of the lens. A stronger curvature of the wavefront is related to a larger divergence of the sound beam. The time delay is measured under each element at a constant depth of $30\,\mathrm{mm}$ and the delay profile across the array is shown in Fig. 5 for the column elements. A similar plot is obtained for the rows but is not shown here. The measurement without a lens (black line) showcases a flat delay profile as opposed to the ones with diverging lenses, which show a larger delay at the edge than in the center of the array. The focal distance F of a lens corresponds to the radius of the circle fitting the data shown in Fig. 5 after conversion of the axis units into distance. To do so, first, the time delay profile is multiplied by the speed of sound in water to obtain a delay distance profile. Secondly, the emitting element numbers are multiplied by the pitch to get the corresponding emitting positions. A circle is fit on the rescaled data and the focal distance F is estimated. The $f_\#$ is deducted and the FOV evaluated using (1). The FOVs measured from the delay profiles are presented in Table II as $FOV_{f_\#}$.

However, the FOV defined by (1) describes the physical limit angle imposed by diffraction but fails to account for the attenuating effect of the lenses. Yet, a signal can only be used for beamforming if its SNR is sufficiently large. Therefore, the usable FOV might be reduced when taking into account the pressure field amplitude. Thus, the effective FOV can be defined by the angle between the axial direction and the $-3\,\mathrm{dB}$ cut-off line from the maximum transmit pressure at each depth as shown in Fig. 1. The experimental FOVs measured from the $-3\,\mathrm{dB}$ contour are also presented in Table II as FOV_{-3dB}.

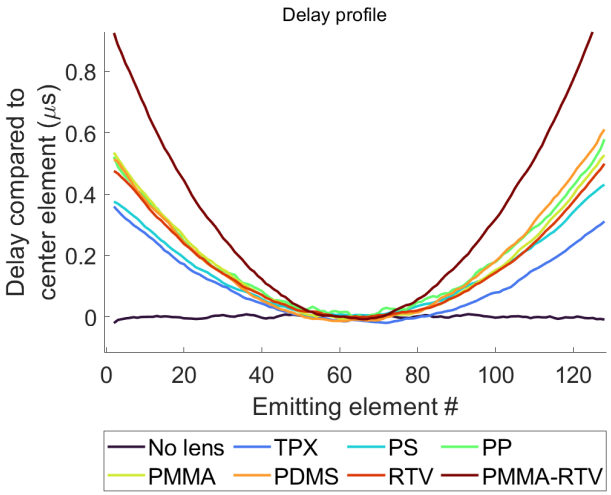

Fig. 5. Measured delay profiles of the different lenses. The profile is built by measuring the signal's arrival time under each element at a constant depth of $30\,\mathrm{mm}$. The delays are plotted relatively to the delay below the center element of the array for better visual comparison. The delay profile is flat when no lens is mounted (black line) and convex when a diverging lens is used (colorful lines). The asymmetry of the parabolic curves might be due to the lens being slightly misaligned.

It is therefore interesting to notice that PDMS appears to have both the largest FOV when calculated from the delay profile and the smallest when calculated from the amplitude pressure map. This is because PDMS has one of the largest acoustic refractive index n_a, but also the largest attenuation α

and a concave lens shape. Therefore, combining both methods enables to properly assess the extent of the volume in which acoustic energy will be found, and in sufficient magnitude. From that matter, it seems that thermoplastic lenses in which the speed of sound is very high provide a significant increase in the usable FOV. The largest FOVs for simple lenses reach $12.2°$ for PMMA, $11.7°$ for PP and $8.1°$ for PS. The largest FOV ($24°$) is obtained with a PMMA-RTV compound lens of $R = 42.64\,\mathrm{mm}$, which results in an imaging area of 6x6 cm^2 at an $8\,\mathrm{cm}$ depth with a 2.5x2.5 cm^2 transducer footprint. The imaging area covered by the transducer is multiplied by 6 at this depth, which greatly improves the potential of the 2D RCA probe for making volumetric anatomical imaging. The value of these FOVs remains far from the usual FOVs of commercial convex transducers [8]–[10]. This is because the lens has been designed to cover a large array ($25.6\,\mathrm{mm}^2$) and constrained to remain relatively thin ($4\,\mathrm{mm}$) therefore imposing a large lower limit on the radius of curvature which is the main parameter driving the FOV. Therefore, to obtain an even larger FOV further optimization of the lens geometry should be performed by using a different surface shape better suited for square footprint transducers [24]. However, this study aims at comparing the performance of different materials, and the method and results would still hold for a different lens geometry designed to reach a higher target FOV.

The potential of these lenses to be used on large high frequency RCA transducers can be investigated through the analysis of the impulse response of the broadband $6\,\mathrm{MHz}$ array used in this study. The impulse response of the lensed array is shown in Fig. 6 for the different lenses. The amplitude drop of the transmit impulse responses in the time domain is calculated in dB using the signal without lens as a reference and is summarized in Table II. The pressure drop is stronger for the convex lenses, which are thicker and therefore more attenuating at the center of the array. A stronger amplitude reduction is also observed for materials with high attenuation coefficient α_0 at the center frequency $f_0 = 6\,\mathrm{MHz}$ like PDMS and PP. A low amplitude will reduce the SNR of the image and will ultimately degrade the penetration depth. Moreover, a strong impedance mismatch also decreases the amplitude of the transmitted signal due to internal refractions. This effect is seen with the PMMA lens ($Z = 3.22$ MRayl, $\alpha_0 = 7.1\,\mathrm{dB\,cm^{-1}}$) for which the amplitude of the response is smaller than for the TPX lens ($Z = 1.69$ MRayl, $\alpha_0 = 10.5\,\mathrm{dB\,cm^{-1}}$) despite having a lower attenuation coefficient at the center frequency of the probe. The impedance and attenuation coefficient both influence the amplitude of the impulse response by around the same order of magnitude and therefore a trade-off might be required, since the best impedance-matched materials (PDMS, TPX) are not the ones with the lowest attenuation (PS, PMMA). These results show the importance of these two parameters in the choice of the lens material to preserve the SNR and image quality when lensing the array. However, it is possible to compensate to some extent for the degraded SNR by using a higher excitation voltage or coded excitation to increase the signal strength [25].

The impulse response in the frequency domain is shown in Fig. 6.b) for the different lensed arrays. The center frequency

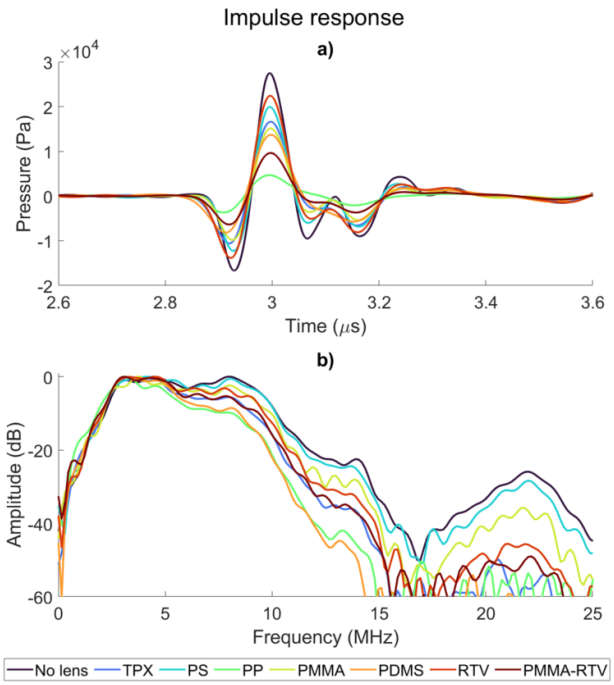

Fig. 6. Measured impulse response in time and frequency domain for the different lenses. The frequency spectrum is normalized according to the measurement without a lens.

of the impulse response is calculated as :

$$f_c = \frac{\sum_{i=0}^{N/2} S(if_s/N) * if_s/N}{\sum_{i=0}^{N/2} S(if_s/N)} \tag{8}$$

where f_c is the center frequency, f_s the sampling frequency, S the FFT of the impulse response and N the number of frequency bins in the two-sided spectrum. The $-3\,\mathrm{dB}$ bandwidth is then calculated as a percentage of the center frequency. The center frequency and bandwidth are summarized in Table II. The acoustic attenuation of polymers increases exponentially with frequency in the MHz range, which translates into a steeper slope in the frequency domain for highly frequency-dependant attenuating materials (large α_f). This highly reduces the bandwidth and causes a down-shift in the center frequency, which will affect negatively the resolution of the image. It can be seen that materials like PDMS and PP damp the signal by more than $30\,\mathrm{dB}$ above $12\,\mathrm{MHz}$. This indicates that the drop in amplitude visible in Fig. 6.a) would be even more dramatic when using a high-frequency transducer ($\geq 10\,\mathrm{MHz}$), and most of the signal will be attenuated after passing through the lens.

The impact of the lenses in terms of potential image artefacts is investigated through the study of secondary echoes in the RF signals as they can give rise to ghost echoes and reverberation artefacts in the beamformed image. The RF signal measured below the center of the array at a $35\,\mathrm{mm}$ depth is shown for the different lenses in Fig. 7 when emitting a plane wave through the lens.

First, it can be seen that all signals showcase a main signal followed by eventual secondary echoes. Fig. 7.a) shows the

measurement without a lens and it is seen that the signal contains a main pulse followed by a second one about $2\,\mu s$ later and whose amplitude is $-15.4\,dB$ of that of the main pulse. The delay of this echo matches the expected position of the edge waves for this array, and this is further confirmed by the fact that this delay varies with depth (shown in Appendix in Fig. 9). The edge waves are due to the finite length of the emitting elements and are expected since the array is not apodized. Edge waves are also visible on the lensed arrays but their relative amplitude compared to the main signal decreases when adding an attenuating polymer lens (from $-15.4\,dB$ without lens down to $-20.9\,dB$ for the PDMS lens).

Moreover, due to the acoustic impedance mismatch between the lens material(s) and the water, the sound is partly reflected at the lens-water interface, which gives rise to another set of secondary echoes after about $5\,\mu s$ and is clearly visible for the PS, PMMA and PMMA-RTV compound lens on Fig. 7.c), e) and h) respectively. The refracted signal amplitude is only $-8.6\,dB$ lower than the main signal for PS, $-10.4\,dB$ for PMMA, and $-10.2\,dB$ for PMMA-RTV. This might introduce large reverberation artefacts in the image making these lenses unsuitable for good image quality. However, these refracted waves could be limited by introducing a matching layer on top of the lens and this should be investigated in a further study.

It is also interesting to notice that despite PP and PS having a similar impedance (2.26 MRayl and 2.42 MRayl), the PS lens showcases very strong refracted echoes, whereas it is completely absent in the PP case. This is because PP is very attenuating and therefore the reflected signal is completely damped during the additional round trip inside the lens, while it is not the case in the low attenuating PS lens. Therefore, highly attenuating materials are found to be beneficial in reducing the relative amplitude of secondary echoes and therefore limiting reverberation and edge wave artefacts. However, they degrade the SNR due to a decrease of the main signal amplitude, and therefore choosing a trade-off towards low to mildly attenuating materials could be preferred.

Finally, B-mode images of a multi-wire phantom are recorded for the simple convex lenses and are shown in Fig. 8 in a $40\,dB$ dynamic range. The results are presented for the TPX lens which exhibits the smallest $FOV_{f\#}$ and best impedance match, and for the PMMA lenses, which has the largest $FOV_{f\#}$ and the worst impedance match. The other lenses, displaying intermediate results, are not included here. The phantom images obtained with the lenses in Fig. 8.b)-c) enable to visualize wire phantoms placed further out compared to the case without a lens in Fig. 8.a). These images thereby confirm that the FOV is increased when using a lens. The measured FOV is represented by the yellow dashed lines and the extent of the array by the red dashed lines. The FOV is more efficiently increased when using a PMMA lens due to the refractive index being larger in PMMA compared to TPX. However, as expected, some artefacts can be seen in the three images, including on the case without a lens. The edge waves in the non-apodized array are responsible for the smaller echo below the main signal pointed out by the white arrow in Fig. 8.a). Additional artefacts are visible in the images obtained with the lenses. In particular, for the PMMA lens, a large number of reverberations are visible and are due to the large impedance mismatch. This considerably degrades the image quality. Finally, it can be seen that the PSF is widely increased when adding a lens. However, the resolution of the image depends on the accuracy of the prediction of the time of flight, which is here calculated based on the thin lens model. To improve the resolution, further development of the beamformer for lensed RCA arrays should be performed but this is beyond the scope of this study. Overall, these images confirm the potential for lenses to increase the FOV of large RCA arrays and also demonstrate their current limitation arising from the material parameters and complexity of beamforming.

A comparison of the advantages and limits of the different polymer lenses is summarized in Table III. Thermoplastics of interest for this application include TPX, PS, PP, and PMMA, in which the speed of sound is higher than in tissue. This enables the fabrication of convex diverging lenses, which are better suited for clinical studies than the concave PDMS and RTV ones. The diverging efficiency of a lens is quantified in terms of FOV and is driven primarily by a large difference in the speed of sound in the material compared to the imaging medium. This appears limiting for some of the polymers studied here (TPX, PS). Furthermore, some thermoplastics have a low frequency-dependent attenuation coefficient (PS, PMMA), which helps preserve the image quality by demonstrating a large bandwidth and making them viable candidates for lensing high-frequency RCA transducers. However, their low attenuation and large impedance mismatch enhance some ghost or reverberation artefacts. Overall, none of the materials simultaneously optimizes all parameters, and trade-offs are necessary. Therefore, the design needs to be optimized specifically for each application as the importance of each requirement might change. Manufacturing a compound lens helps combine the beneficial effects of several materials and double the FOV but also suffers from increased attenuation and artefacts.

V. Conclusion

This work presented a new method for fabricating custom-made acoustic lenses in a fast, cost-effective, and flexible manner. Indeed, the fabrication process enables many variations of the dimensions and shape of the lens (concave, convex, compound, single or double curved lens). The flexibility in the geometry is provided by the use of a combination of 3D printing, casting, and CNC machining techniques. The recent improvements in these techniques now allow for the manufacturing of pieces with a sub-wavelength resolution, necessary for making such acoustic lenses. In particular, the micro-milling manufacturing technique opens the path for using a new range of materials for acoustic lenses. While casting remains the preferred manufacturing method for thermosetting polymers, micro-milling is found optimal for shaping thermoplastics.

Using thermoplastics polymers enabled the fabrication of a diverging spherical convex lens for a large aperture $6\,MHz$ RCA transducer. These simple convex lenses made of TPX,

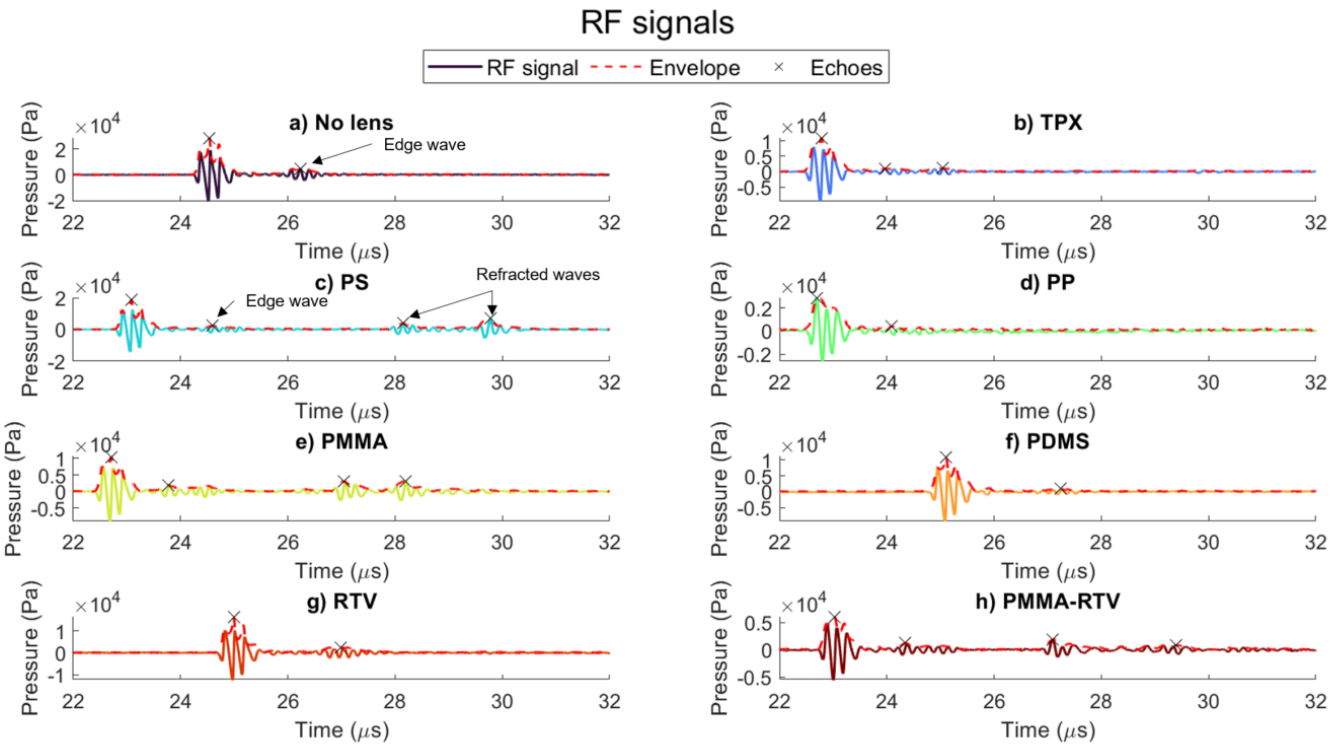

Fig. 7. RF signals measured at position [0,0,35] mm for different lenses. a) shows the case without a lens for reference. b)-e) are measured on convex lenses, f)-g) on concave lenses, and h) on the compound lens. The y-axis scales differently on each graph. The main signal is followed by an edge wave with a 2 µs delay. When adding an attenuating polymer lens, the absolute amplitude of the main echo severely decreases, but so does the relative amplitude of the edge wave compared to the main signal. Due to acoustic impedance mismatch between the lens material and the water, the sound is partly reflected at the lens interface, which gives rise to another set of secondary echoes clearly visible on c), e), and h). The amplitude of the largest secondary echo compared to the main signal is presented in Table II.

Summary of the performances of the lenses

Parameter	Requirement	Material parameter(s) involved	Lens material						
			TPX	PS	PP	PMMA	PDMS	RTV	PMMA-RTV
Lens shape	Flat or convex surface	v_l	+	+	+	+	-	-	++
FOV	Large	v_l	-	-	+	+	-	+	++
SNR at high frequency	Large	α, α_f, Z	+	+	-	+	-	+	-
Bandwidth	Large	α_f	-	+	-	+	-	-	-
Artefacts	Small ghost and reverberation artefacts	Z	+	-	+	-	+	+	-

TABLE III
QUALITATIVE COMPARISON OF THE IMAGING PERFORMANCE OF THE DIFFERENT LENSES. $(+)$ DENOTES A GOOD PERFORMANCE FOR THAT PARAMETER AND $(-)$ A NEGATIVE ONE. NONE OF THE MATERIAL OPTIMIZES SIMULTANEOUSLY ALL PARAMETERS.

PS, PP or PMMA increase the FOV by a maximum of 12.2° for PMMA which, however, is still far from the value of commercial convex arrays. Using a combination of PMMA and RTV in a compound lens proved to be promising by increasing the FOV up to 24°. The FOV could be further increased by optimizing the geometry of the lens with a different surface shape [24]. Moreover, some of these materials (PS, PMMA) have demonstrated their ability to preserve the bandwidth and a high SNR at high frequency, which makes them suitable materials to lens high-frequency transducers. However, one challenge still remains to limit the artefacts arising from the secondary echoes generated at the water-lens interface, which are due to the acoustic impedance mismatch of the lens material. Building a matching layer on top of the lens or tuning the impedance of the polymer by using composites of different densities could be ways to overcome this issue but are beyond the scope of this study.

To conclude, this work presented a method to design, fabricate, and characterize several diverging lenses made of various materials and geometries. The lenses have been fabricated and their characterization has demonstrated their potential to improve volumetric anatomical imaging using large aperture high-frequency 2D RCA transducers while preserving the image quality.

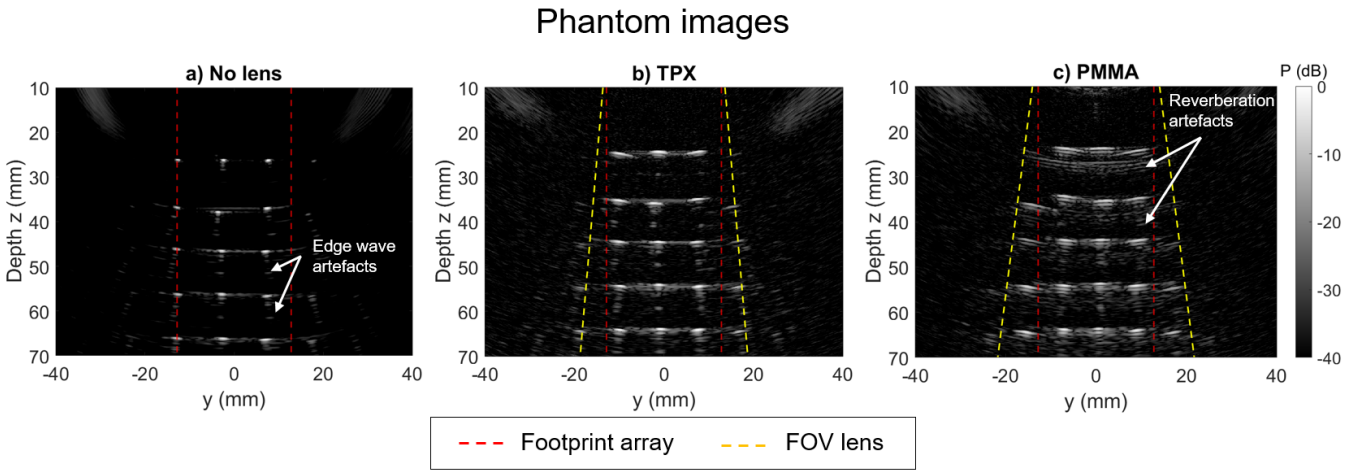

Fig. 8. B-mode images of a multi-wire phantom placed along the y-axis with a 40 dB dynamic range. The yellow dashed lines represent the extent of the measured FOV, and the red dashed lines the extent of the array. The FOV is increased when adding a lens, as seen by the increased number of visible wires. The arrows point at some artefacts generated by the edge waves of the RCA array and the internal reflections caused by the lens material impedance mismatch.

ACKNOWLEDGMENT

The work is supported by the European Research Council's (ERC) Synergy Grant 854796.

REFERENCES

[1] C. E. Morton and G. R. Lockwood, "Theoretical assessment of a crossed electrode 2-D array for 3-D imaging," *Proc. IEEE Ultrason. Symp.*, vol. 1, D. E. Yuhas and S. C. Schneider, Eds., 968–71 vol.1, 2004.

[2] A. Stuart Savoia, B. Mauti, L. Fanni, *et al.*, "A 120+ 120- Element Crisscross CMUT Probe's with Real-Time Switchable Electronic and Fresnel Focusing Capabilities," *Proc. IEEE Ultrason. Symp.*, vol. 2018-, p. 8 580 084, 2018.

[3] R. Chee, A. Sampaleanu, D. Rishi, and R. Zemp, "Top orthogonal to bottom electrode (TOBE) 2-D CMUT arrays for 3-D photoacoustic imaging," *IEEE Trans. Ultrason., Ferroelec., Freq. Contr.*, vol. 61, no. 8, pp. 1393–1395, 2014.

[4] J. A. Jensen, M. Schou, L. T. Jørgensen, *et al.*, "Anatomic and Functional Imaging using Row-Column Arrays," *IEEE Trans. Ultrason., Ferroelec., Freq. Contr.*, vol. 69, no. 10, pp. 2722–2738, 2022.

[5] M. F. Rasmussen and J. A. Jensen, "3D ultrasound imaging performance of a row-column addressed 2D array transducer: a simulation study," *Proc. SPIE - Int. Soc. Opt. Eng.*, vol. 8675, p. 86750C, 2013.

[6] C. H. Seo and J. T. Yen, "A 256 × 256 2-D array transducer with row-column addressing for 3-D rectilinear imaging," *IEEE Trans. Ultrason., Ferroelec., Freq. Contr.*, vol. 56, no. 4, p. 4 815 314, 2009.

[7] J. Sauvage, J. Poree, C. Rabut, *et al.*, "4D Functional Imaging of the Rat Brain Using a Large Aperture Row-Column Array," *IEEE Trans. Med. Imag.*, vol. 39, no. 6, pp. 1884–1893, 2020.

[8] GE Healthcare, "Curved array Vscan Air," General Electric Company, Tech. Rep., 2021. [Online]. Available: https://www.gehealthcare.com/-/media/A66296638B1D4D4EA4B9411857A38066.pdf.

[9] S. H. A. Juniper, "Curved array transducer 8VC3," Siemens Healthcare GmbH, Tech. Rep., 2021. [Online]. Available: https://www.siemens-healthineers.com/ultrasound/ultrasound-transducer-catalog.

[10] Phillips, "Curved array transducer C5-2," Philips North America Corporation, Tech. Rep., 2021. [Online]. Available: https://www.usa.philips.com/healthcare/product/HC989605427371/c5-2-usb.

[11] M. Z. Z. P. U. systen, "Convex array C8-33D," Zonare Medical Systems, Tech. Rep. [Online]. Available: https://www.mindraynorthamerica.com/wp-content/uploads/2020/07/Mindray2020_transducers_Z.OnePRO_Final_RevB_.pdf.

[12] H. Bouzari, M. Engholm, C. Beers, *et al.*, "Curvilinear 3-D Imaging Using Row–Column Addressed 2-D Arrays with a Diverging Lens: Phantom Study," *IEEE Trans. Ultrason., Ferroelec., Freq. Contr.*, vol. 65, no. 7, pp. 1182–1192, 2018.

[13] M. Engholm, C. Beers, H. Bouzari, J. A. Jensen, and E. V. Thomsen, "Increasing the field-of-view of row–column-addressed ultrasound transducers: implementation of a diverging compound lens," *Ultrasonics*, vol. 88, pp. 97–105, 2018.

[14] W. Xia, D. Piras, J. C. van Hespen, W. Steenbergen, and S. Manohar, "A new acoustic lens material for large area detectors in photoacoustic breast tomography," *Photoacoustics*, vol. 1, no. 2, pp. 9–18, 2013.

[15] S. Yang, W. Qin, H. Guo, *et al.*, "Design and evaluation of a compound acoustic lens for photoacoustic computed tomography," *Biomed. Opt. Express*, vol. 8, no. 5, pp. 2756–2765, 2017.

[16] S. H. Kim and J. H. Chang, "Effect of Acoustic Properties of Lens Materials on Performance of Capacitive

Micromachined Ultrasonic Transducers," *J. Med. Biol. Eng.*, vol. 36, no. 4, pp. 536–544, 2016.

[17] A. W. Joyce and G. R. Lockwood, "Crossed-array transducer for real-time 3D imaging," *Proc. IEEE Ultrason. Symp.*, p. 6 932 003, 2014.

[18] C. Chang, K. Firouzi, K. Kyu Park, *et al.*, "Acoustic lens for capacitive micromachined ultrasonic transducers," *J. Micromech. Microeng.*, vol. 24, no. 8, p. 085 007, 2014.

[19] P. J. Ernst, "Measurement and Specification of Ultrasonic Lenses," *J. Acoust. Soc. Am.*, vol. 19, no. 3, pp. 474–474, 1947.

[20] S. H. Øygard, M. Audoin, A. Austeng, E. V. Thomsen, M. B. Stuart, and J. A. Jensen, "Accurate prediction of transmission through a lensed row-column addressed array," *J. Acoust. Soc. Am.*, vol. 151, no. 5, pp. 3207–3218, 2022.

[21] M. Engholm, C. Beers, A. S. Havreland, B. G. Tomov, J. A. Jensen, and E. V. Thomsen, "A Row–Column-Addressed 2D Probe with an Integrated Compound Diverging Lens," *Proc. IEEE Ultrason. Symp.*, vol. 2018-, p. 8 579 955, 2018.

[22] H. Wang, W. Jiang, and W. Cao, "Characterization of lead zirconate titanate piezoceramic using high frequency ultrasonic spectroscopy," *J. Applied Phys.*, vol. 85, no. 12, pp. 8083–8091, 1999.

[23] A. Salari, M. Audoin, B. G. Tomov, E. V. Thomsen, and J. A. Jensen, "Increasing penetration depth and field-of-view in 3D ultrasound imaging with Row-Column Array," *Proc. IEEE Ultrason. Symp.*, vol. 2023-, pp. 1–3, 2023.

[24] M. Audoin, A. Salari, B. G. Tomov, J. A. Jensen, and E. V. Thomsen, "Novel Diverging Acoustic Lens Geometries for Row-Column Array Transducers," *Proc. IEEE Ultrason. Symp.*, vol. 2023-, pp. 1–4, 2023.

[25] A. Misaridis, K. Gammelmark, C. H. Jørgensen, *et al.*, "Potential of coded excitation in medical ultrasound imaging," *Ultrasonics*, vol. 38, no. 1-8, pp. 183–189, 2000.

APPENDIX

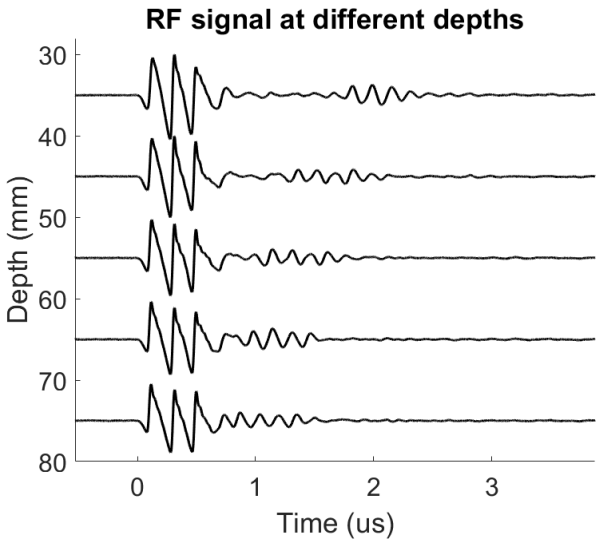

Fig. 9. Normalized RF signals measured at [0,0,z] mm with z varying from 35 to 75 mm for the case without lens. The signals have been re-phased so that the x-axis shows the arrival time after the main signal, for better visual comparison. The secondary echo delay to the main signal decreases with depth, which is expected for an edge wave. The 2 $\mu\mathrm{s}$ delay at 35 mm depth is also expected for a 25.6 mm transducer aperture.